Journal of Colloid and Interface Science 628 (2022) 463–475

Contents lists available at ScienceDirect

Journal of Colloid and Interface Science

journal homepage: www.elsevier.com/locate/jcis

Charge converting nanostructured lipid carriers containing a cell-penetrating peptide for enhanced cellular uptake

Patrick Knoll [a], Nikolas Hörmann [b], Nguyet-Minh Nguyen Le [a], Richard Wibel [a], Ronald Gust [b], Andreas Bernkop-Schnürch [a,*]

[a] Center for Chemistry and Biomedicine, Department of Pharmaceutical Technology, Institute of Pharmacy, Leopold-Franzens-University of Innsbruck, Innrain 80/82, 6020 Innsbruck, Austria
[b] Center for Chemistry and Biomedicine, Department of Pharmaceutical Chemistry, Institute of Pharmacy, Leopold-Franzens-University of Innsbruck, Innrain 80/82, 6020 Innsbruck, Austria

GRAPHICAL ABSTRACT

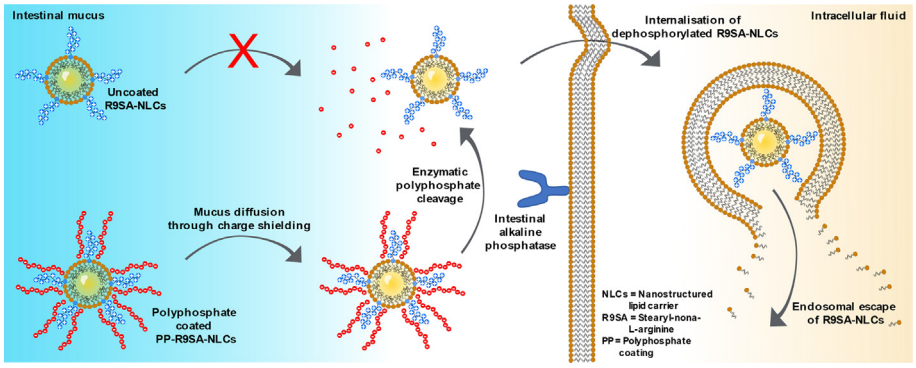

ARTICLE INFO

Article history:
Received 6 May 2022
Revised 11 July 2022
Accepted 26 July 2022
Available online 29 July 2022

Keywords:
Nanostructured lipid carrier
Charge conversion
Cell-penetrating peptide

ABSTRACT

Hypothesis: The aim of this study was the development of nanostructured lipid carriers (NLCs) decorated with a polycationic cell-penetrating peptide (CPP). A coating with polyphosphates (PP) enables charge conversion at target cells being triggered by the membrane bound enzyme intestinal alkaline phosphatase (IAP).

Experiments: The CPP, stearyl-nona-L-arginine (R9SA) was obtained by solid phase synthesis. Formed nanocarriers were characterized regarding size, polydispersity index, zeta potential and charge conversion in the presence of IAP and on Caco-2 cells. The BCS class IV drug saquinavir (SQV) was loaded into NLCs in different concentrations. Mucus diffusion ability of the NLCs was evaluated by the rotating tube method. Furthermore, cellular uptake was evaluated on Caco-2 cells and endosomal escape properties were investigated using erythrocytes.

Abbreviations: NLCs, nanostructured lipid carriers; CPP, cell-penetrating peptide; IAP, intestinal alkaline phosphatase; R9SA, stearyl-nona-L-arginine; PP, polyphosphate; blank NLC, nanostructured lipid carriers without stearyl-nona-L-arginine; R9SA-NLC, stearyl-nona-L-arginine loaded nanostructured lipid carriers; PP-R9SA-NLC, polyphosphate coated stearyl-nona-L-arginine loaded nanostructured lipid carriers; 2-CTC, 2-chlorotritylchloride resin; DIC, N,N-diisopropylcarbodiimide; HOBT, 1-hydroxybenzotriazol; TFA, trifluoroacetic acid; MALDI-TOFMS, matrix-assisted laser desorption/ionization time-of-flight mass spectrometry; DCM, dichloromethane; DMF, N,N-dimethylformamide; DIPEA, N,N-diisopropylethylamine; SQV, saquinavir; FaSSIF, fasted-state simulated intestinal fluid; SIF, simulated intestinal fluid; SGF, simulated gastric fluid; DLS, dynamic light scattering; MEM, minimum essential medium; FBS, fetal bovine serum; LGR, Lumogen red; HBS, HEPES buffered saline; PIC2, phosphatase inhibitor cocktail 2; PBS, phosphate buffered saline; FSC-A, area of forward scatter; SSC-A, area of side scatter.

* Corresponding author.
E-mail address: Andreas.Bernkop@uibk.ac.at (A. Bernkop-Schnürch).

https://doi.org/10.1016/j.jcis.2022.07.160

Cellular uptake
Endosomal escape
Polyarginine
Nanocarriers
Saquinavir

Findings: All NLCs were obtained in a size range between 146 nm and 152 nm and a polydispersity index of 0.2. Incubation of PP coated PP-R9SA-NLCs with IAP led to a charge conversion from −41.8 mV to 6.4 mV (Δ48.2 mV). After four hours of incubation with IAP, phosphate release reached a plateau, indicating a faster polyphosphate cleavage than on Caco-2. Drug load and encapsulation efficiency of SQV was obtained up to 80.6% and 46.5 μg/mg. Mucus diffusion was increasing in the following rank order: R9SA-NLCs < blank NLCs < PP-R9SA-NLCs. R9SA-NLCs and PP-R9SA-NLCs increased the cellular uptake 15.6- and 13.2-fold, respectively, compared to the control NLCs. Erythrocytes interaction study revealed enhanced endosomal escape properties for R9SA-NLCs and PP-R9SA-NLCs when incubated with IAP.

1. Introduction

Nanostructured lipid carriers (NLCs) are lipid-based formulations that can be utilized for oral administration of various types of drugs. Especially highly lipophilic BCS class II or IV drugs such as tamoxifen, tacrolimus, vinpocetine and saquinavir were loaded into NLCs to increase their bioavailability [1-4]. So far, however, NLCs have not reached their full potential as various hurdles such as enzymatic degradation during gastrointestinal transit, permeation through the mucus gel barrier and poor cellular uptake still have to be mastered [5]. In particular sound strategies to overcome the mucus gel barrier and the limited uptake by epithelial cells seem to be key to success. Since the main organic components of mucus are mucins, consisting of highly glycosylated proteins with sialic and sulfonic acid moieties, the mucus environment is predominantly negatively charged [6]. Therefore, NLCs bearing a polycationic surface show strong interactions with mucins reducing mucus permeation and consequently also the number of nanocarriers reaching the absorption membrane [7]. Accordingly, a polyanionic surface of NLCs is advantageous to provide high mucus permeating properties. Having reached the underlying epithelial cell layer, however, a polycationic surface is needed, which is essential for high internalization into cells [8]. One approach to address this so-called polycation dilemma is the coating of the polycationic surface of NLCs with polyphosphates (PP) in order to reduce interactions with the mucus [9]. Effective mucus permeation of phosphate-bearing nanocarriers has been demonstrated in previous studies [10,11]. The brush border associated enzyme alkaline phosphatase cleaves the PP as soon as the carrier has reached the epithelium, resulting in a conversion of the surface charge from negative to positive [12]. In order to provide a polycationic surface of NLCs, favoring cellular uptake, in particular cationic cell-penetrating peptides (CPP) are advantageous [13]. Le *et al.* recently provided evidence for the enhanced uptake of poly-L-lysine decorated nanoemulsions on Caco-2 cells [14]. Since polyarginine was shown to be an even more effective CPP for pDNA transport than polylysine [15], it might strongly improve the cellular uptake of NLCs. Coating polyarginine-decorated NLCs with PP, furthermore, might lead to NLCs that on the one hand can efficiently permeate the mucus gel layer and, on the other hand, provide high cellular uptake.

Based on this concept, NLCs bearing polyarginine moieties on their surface that are coated with PP were developed and characterized in this study. NLCs were decorated with stearyl-nona-L-arginine (R9SA) and coated with PP. NLCs without R9SA (blank NLCs), with R9SA (R9SA-NLCs), and with polyphosphate coating (PP-R9SA-NLCs) were evaluated regarding their size, polydispersity index, zeta potential and stability in different biorelevant media. Furthermore, the BCS class IV drug saquinavir was loaded in different concentrations into the NLCs, which were evaluated regarding drug load and encapsulation efficiency. Charge conversion was investigated after incubation with intestinal alkaline phosphatase (IAP), phosphate release after incubation with isolated and cell membrane-bound IAP. Mucus diffusion properties of NLCs were determined by a rotating tube assay. Furthermore, cellular uptake on Caco-2 cells was determined photometrically and by flow cytometry after cytocompatibility of NLCs was shown. In addition, endosomal escape properties were investigated by interaction studies with erythrocytes.

2. Materials and methods

2.1. Materials

Nona-L-arginine (≥98%) was purchased from Shanghai Hanhong Chemical Co. (Shanghai, China). Acetone was obtained from DonauChem (Vienna, Austria). Lumogen red (LGR) was a kind gift from BASF (Ludwigshafen, Germany). Miglyol® 840 (middle-chain triglycerides) was received by IOI Oleo GmbH (Witten, Germany). 4-(2-Hydroxyethyl)-1-piperazineethanesulfonic acid (HEPES, ≥ 99.5%) and *N*,*N*-dimethylformamide (DMF, ≥ 99.5%) was obtained from Roth GmbH (Karlsruhe, Germany). Precirol ® ATO 5 (glyceryl distearate) was a free sample from Gattefossé (St. Priest, France). D-Glucose anhydrous (≥99.5%), sodium chloride (≥99.5%), and acetonitrile (≥99.5%) was received from VWR Chemicals (Solon, USA). Phosphate buffered saline (PBS), penicillin, streptomycin, and fetal bovine serum (FBS) were obtained from Merck (Tutzing, Germany). Lipoid S100 (soy lecithin) was a gift from Lipoid GmbH (Ludwigshafen, Germany). Alkaline phosphatase from bovine intestinal mucosa (≥10 DEA U/mg), ammonium molybdate tetrahydrate (81.0–83.0%), magnesium chloride anhydrous (≥98%), sodium polyphosphate (Graham's salt, ≥ 99.7%), zinc chloride anhydrous (≥97%), potassium phosphate monobasic (KH_2PO_4, ≥ 99%), phosphatase inhibitor cocktail 2, Triton X-100, malachite green oxalate salt (MLG), minimum essential medium eagle (MEM), resazurin sodium salt, stearic acid (≥98.5%), trypan blue (0.4%), trifluoroacetic acid (99%), 1-hydroxybenzotriazol (HOBT, ≥ 97%), dichloromethane (DCM, ≥ 99.8%), N,N-diisopropylethylamine (DIPEA, ≥ 99.5%), pepsin from gastric mucosa and pancreatin from porcine pancreas were purchased from Sigma-Aldrich (Vienna, Austria). Saquinavir was obtained from Biosynth (Staad, Switzerland). FaSSIF powder was received from Biorelevant (London, U.K.).

2.2. Synthesis of R9SA

Peptide coupling was performed by a standard solid-phase synthesis procedure on a 2-chlorotritylchloride resin (2-CTC; loading capacity 1.6 mmol/g; Iris Biotech GmbH, Marktredwitz, Germany) using a peptide synthesis vessel. Anhydrous reactions were performed under an inert argon atmosphere, using oven-dried glassware and syringes to add substances. The resin (173 mg) was swollen for 30 min in 3 mL of dichloromethane (DCM) at room temperature. Nona-L-arginine (150 mg, 0.10 mmol) was dissolved in *N*,*N*-dimethylformamide (DMF; 10 mL/g resin), and pH was

adjusted to 8 with *N*,*N*-diisopropylethylamine (DIPEA). After washing the resin three times with DCM, the peptide solution was loaded onto the resin and coupled for at least 2 h. Then, the remaining binding sites of the resin were capped with methanol/DIPEA/DMF in a ratio of 500 µL/250 µL/800 µL for 30 min. The reaction solution was removed by filtration, and the resin was washed twice with DCM and twice with DMF. To a solution of stearic acid (148 mg, 0.52 mmol) in 5 mL of DMF (pH adjusted to 8 with DIPEA), *N*,*N*-diisopropylcarbodiimide (DIC; 89 µL, 0.57 mmol) was added slowly while stirring for another 10 min, followed by the addition of 1-hydroxybenzotriazol (HOBT; 88 mg, 0.57 mmol) in 2 mL of DMF. The suspension was then loaded onto the resin, and coupling was performed for at least 5 h. After washing the peptide-resin three times with 3 mL of DMF and then three times with 3 mL of DCM, the solvent was removed through filtration. The dried peptide-resin was separated for one hour using a mixture of TFA/DCM (70/30, *v/v*). The crude peptide was precipitated in an ice-cold mixture of 5 mL of acetonitrile/water (1/1, *v/v*). After centrifugation, the supernatant was removed, and the crude residue was purified by RP-HPLC. Purification was set up on a GILSON 322 preparative chromatography system with a GILSON UV/VIS-155D multi-wavelength UV detector. Gradient elution was performed on an Eurosil Bioselect 300-5 C18 A column (Vertex Plus, 300 × 8 mm, Knauer, Berlin, Germany), combined with an Eurosil Bioselect 300-5 C18 precolumn, using a water/acetonitrile/0.1% TFA gradient. The final product was freeze-dried and stored at −20 °C until further use.

2.3. HPLC and mass spectrometry

Analytical HPLC was performed using an UltiMate 3000 chromatography system, equipped with a Phenomenex Jupiter 4 µm Proteo 90 Å C12 column, 250 × 4.6 mm (Phenomenex Ltd., Aschaffenburg, Germany) and analysed with Chromeleon Dionex Software (Version 7.2.9.11323). Detection wavelength (UV) was set at λ = 220 nm. The molecular weight of the final product was confirmed by a matrix-assisted laser desorption/ionization-time-of-flight (MALDI-TOF MS) mass spectrometer (Bruker Daltonics, Bremen, Germany).

2.4. Preparation of NLCs

R9SA-NLCs were prepared using a solvent diffusion method, as previously described, with some modifications [16]. Briefly, 50 mg of glyceryl distearate, 50 mg of middle-chain triglycerides and 50 mg of soy lecithin were dissolved in 5 mL of acetone at 40 °C using a thermomixer (ThermoMixer C, Eppendorf Vertrieb Deutschland GmbH, Germany). The aqueous phase was assembled by 0.5 mg of R9SA dissolved in 800 µL of demineralized water. The lipid phase and the aqueous phase were heated to 40 °C and mixed at 1000 rpm. After adding 100 µL of lipid phase to the R9SA solution, the mixture was shaken at 1000 rpm for 25 min to evaporate acetone. Formed NLCs were cooled down on ice and stored in the refrigerator until further use.

Blank NLCs were prepared in the same way as described above, without loading R9SA into NLCs. To obtain a comparable size and polydispersity index as for R9SA-NLCs, blank NLCs were sonicated using a Hielscher UP200H (Hielscher, Teltow, Germany) at an amplitude of 80% and 0.5 Hz for 2.5 min.

Phosphate coated NLCs, hereafter referred to as PP-R9SA-NLCs, were obtained by adding the polyphosphate Graham's salt in a molar ratio of polyphosphates to R9SA of 1.5:1 to R9SA-NLCs. The degree of polymerized phosphates in Graham's salt is reported by the manufacturer to be 25 phosphates per molecule. All nanocarriers were labeled with Lumogen red (LGR) by dissolving 0.5% (*m/v*) LGR in the lipid phase of NLCs.

2.5. Nanocarrier size, polydispersity index (PDI) and zeta potential

Size, PDI, and zeta potential of NLCs were measured by photon correlation spectroscopy using Zetasizer Nano ZS (Malvern Instruments, UK). Therefore, nanocarriers were diluted to a final concentration of 0.01% (*m/v*) with demineralized water. Size and polydispersity index were determined with a backscatter angle of 173° by a He-Ne laser at 633 nm. Zeta potential was measured using a dip cell (Malvern Instruments, Malvern, U.K.) at a scattering angle of 12.8°. All investigations were performed at 37 °C in triplicate.

2.6. Preparation and characterization of saquinavir loaded NLCs

Nanocarriers were loaded with saquinavir (SQV) as BCS class IV model drug. NLCs were prepared as described above dissolving SQV in concentrations of 3%, 6% and 9% (*m/v*) in the lipid phase. NLCs were evaluated for size, PDI, zeta potential, drug load, and encapsulation efficiency. Information on size, PDI, and zeta potential were obtained by a zetasizer as described above. To determine the encapsulation efficiency and the drug load, 200 µL of NLC dispersion were centrifuged at 3,000 g at 4 °C for 20 min using Amicon® centrifugal filters (Merck, Tutzing, Germany) with a molecular weight cut-off of 100 kDa. The unencapsulated SQV in the filtrate was analyzed by HPLC. An Elite LaChrom HPLC was equipped with a KNAUER Eurospher 100-5 reverse phase C18 column with precolumn (250 × 4 mm, 5 µm) as the stationary phase, as well as a L-2130 pump, an L-2450 diode array detector (VWR Hitachi, Vienna, Austria) and an L-2200 autosampler. The mobile phase consisted of a mixture of 0.1% TFA/acetonitrile (60/40, *v/v*). SQV was detected at a wavelength of 354 nm after an elution time of 3.7 min. A calibration curve was created ranging from 0.001 to 100 µg/mL ($R^2 > 0.99$) to quantify SQV. The injection volume was set to 50 µL and the total time of the analysis run was 10 min. The drug load was calculated by the following equation:

$$\text{Drug load}\ (\mu g/mg) = \frac{\textit{total amount of drug} - \textit{unencapsulated amount of drug}}{\textit{total lipid content}}$$

The encapsulation efficiency was calculated as follows:

$$\text{Encapsulation efficiency}\ (\%) = \frac{\textit{total amount of drug} - \textit{unencapsulated amount of drug}}{\textit{total amount of drug}}$$

2.7. Stability in simulated biorelevant fluids

NLCs were evaluated for stability in biorelevant media including fasted-state simulated intestinal fluid (FaSSIF), simulated intestinal fluid (SIF) with and without pancreatin, and simulated gastric fluid (SGF) with and without pepsin. FaSSIF was prepared as described by the manufacturer. SIF was prepared with and without 0.4% (*m/v*) pancreatin, whereas SGF was prepared with and without 0.32% (*m/v*) pepsin according the USP. NLCs were dispersed in a final concentration of 0.01% (*m/v*) with each buffer and analyzed *via* dynamic light scattering (DLS) as described above. Size and PDI of NLCs were determined directly and after 4 h incubation at 37 °C. The impact of phosphate cleavage was evaluated by adding IAP at a final concentration of 1 U/mL.

2.8. Phosphate release and zeta change after incubation with IAP

Phosphate release of phosphate-coated PP-R9SA-NLCs was investigated after cleaving the phosphate coating by intestinal alkaline phosphatase (IAP) as described previously [17]. In brief,

1 mL of 0.01% (*m/v*) PP-R9SA-NLCs was prepared in 100 mM HEPES containing 5 mM $MgCl_2$ and 0.2 mM $ZnCl_2$. Phosphate cleavage was initiated by adding 1 µL of a 1000 U/µL IAP solution to obtain a final concentration of 1 U/mL IAP. Samples were incubated at 37 °C and 300 rpm for 240 min. Aliquots of 50 µL were withdrawn at predetermined time points and transferred to a 96 well plate. Enzymatic activity was stopped with 5 µL of 3.6 M sulfuric acid. PP-R9SA-NLCs samples without IAP were treated similarly and served as control. Quantification of phosphate release was performed under the aid of a calibration curve of increasing dilutions of KH_2PO_4 solution. Free phosphate was determined photometrically at a wavelength of 630 nm (TECAN Spark®, Tecan Group Ltd., Switzerland) after the addition of 100 µL of malachite green reagent.

The zeta potential of PP-R9SA-NLCs was determined after 4 h of incubation with 1 U/mL of IAP using Zetasizer Nano ZS. The nanocarriers were washed twice before measurement with demineralized water by centrifugal concentrator Vivaspin (molecular weight cut off: 100 KDa). The surface charge of NLCs was measured in triplicate using a dip cell.

2.9. Mucus diffusion study

The ability of NLCs to penetrate mucus was investigated by the rotating tube method using silicone tubes filled with porcine small intestinal mucus [21]. For this purpose, silicone tubes from Lactan (Graz, Austria) with an inner diameter of 3 mm were cut into 4 cm long pieces and filled with 150 µL of mucus by a 1 mL syringe. LGR labeled blank NLCs, R9SA-NLCs, and PP-R9SA-NLCs were dispersed to a final concentration of 0.1% (*m/v*) in 50 mM phosphate buffer pH 6.8, and 50 µL of each formulation was added to the mucus inside the tube. After sealing the endings of tubes with parafilm, the tubes were rotated at 37 °C and 50 rpm for 24 h under light protection. The tubes were then frozen at −80 °C and cut into segments of 2 mm length. Each segment was mixed with 250 µL DMF and shaken in a horizontal shaker at 150 rpm for 2 h to extract the LGR from the mucus. After centrifugation for 5 min at 13,400 rpm, fluorescence intensity was determined in the supernatant fluid photometrically at an excitation wavelength of 575 nm and an emission wavelength of 610 nm.

2.10. Cell studies

2.10.1. Cell culturing

Caco-2 cells were seeded in 24 well plates in a density of 2.5×10^4 cells per well in 500 µL of minimum essential medium (MEM) containing 10% (v/v) heat inactivated fetal bovine serum (FBS) and penicillin/streptomycin solution (100 units/0.1 mg/L). Cells were incubated at 37 °C in an atmosphere of 95% relative humidity and 5% CO_2 for 12 days. The medium was changed every two days.

2.10.2. Cytotoxicity evaluation

NLCs were tested for cytotoxic effects on Caco-2 cells prior further cell studies as described previously [18]. Blank NLCs, R9SA-NLCs and PP-R9SA-NLCs were prepared in sterile HEPES buffered saline (HBS) pH 7.4 containing 1 g/L dextrose, 20 mM HEPES, 5 mM KCl, 136.7 mM NaCl, and 1 mM $CaCl_2$ in final concentrations of 0.1% (*m/v*), 0.05% (*m/v*) and 0.01% (*m/v*), respectively. HBS alone served as the negative control, and 0.1% (*v/v*) Triton-X 100 in HBS was used as the positive control. Cells were washed three times with HBS before adding 500 µL of samples. NLCs were incubated on cells for 4 and 24 h. At the end of incubation, nanocarriers were removed and cells were washed three times with HBS. 500 µL of resazurin solution was added at a final concentration of 0.1% (*m/v*) and incubated for 2 h. Aliquots of 100 µL were transferred to a black 96 well plate and fluorescence intensity was determined at an excitation wavelength of 540 nm and an emission wavelength of 590 nm. The viability of cells was calculated according to the following equation:

$$\text{Cell viability}\,(\%) = \frac{\textit{intensity of sample} - \textit{intensity of negative control}}{\textit{intensity of positive control} - \textit{intensity of negative control}} \text{ x } 100$$

2.10.3. Phosphate cleavage by Caco-2 cells

Phosphate cleavage and release of PP-R9SA-NLCs were also investigated on Caco-2 cells [19]. PP-R9SA-NLCs containing 1% phosphatase inhibitor cocktail 2 (PIC2) served as control. Prior to the study, cells were washed three times with prewarmed sterile HBS, and defined wells were incubated for 60 min with HBS and HBS containing 1% (*v/v*) PIC2. The buffer was replaced with 1000 µL of 0.01% (*m/v*) PP-R9SA-NLCs and PP-R9SA-NLCs, including 1% (*v/v*) PIC2. At predetermined time points, 50 µL of each well were withdrawn and transferred in a 96 well plate. Enzyme activity was terminated with 5 µL of 3.6 M sulfuric acid. Time dependent phosphate release was determined photometrically at 630 nm by a malachite green assay. Results were calculated using a calibration curve obtained by dilutions of a KH_2PO_4 solution.

2.10.4. In vitro cellular uptake

Cellular uptake studies of 0.5% (*m/v*) LGR labeled blank NLCs, R9SA-NLCs, PP-R9SA-NLCs and PP-R9SA-NLCs containing 1% (*v/v*) PIC2 were performed on Caco-2 cells. Cells were washed three times with prewarmed HBS. Wells of the control PP-R9SA-NLCs containing PIC2 were treated with 1% (v/v) PIC2 for 60 min before samples were added. After removing the buffer from the cells, 500 µL of nanocarriers were added at a final concentration of 0.01% (*m/v*) in HBS. Following three hours of incubation, samples were removed from cells and the cells were washed three times with phosphate-buffered saline (PBS). Buffer was left on cells after the last washing step. The cells were lysed by adding 100 µL of 4% (*v/v*) Triton-X 100 in PBS to each well and incubating at 37 °C for 30 min in an orbital shaker (Incubator ES-80, Grant Instruments Ltd., Cambridge, England). Fluorescence intensity was measured photometrically at an excitation wavelength of 575 nm and an emission wavelength of 610 nm after transferring 100 µL of each well to a black microtiter plate. Cells treated with NLCs simultaneously and after 3 h incubation without washing served as 100% value. The amount of proteins in each well was determined using the Pierce™ Micro BCA™ assay kit. Bovine serum albumin at various dilutions served as a calibration curve. Cellular uptake was calculated as percentage uptake and as µg NLCs per mg protein.

Cellular uptake was also performed using a flow cytometer (BD LSRFortessa™ Cell sorter). 0.5% (*m/v*) LGR labeled NLCs were incubated on cells in the same concentration and under the same conditions as described above. After washing the cells three times with HBS, cells were detached from wells by the addition of 150 µL trypsin and incubating at 37 °C for 5 min. Trypsin activity was stopped with 400 µL of MEM and cells were separated with a pipette for 30 s. The suspensions containing single cells from two wells were combined in a 15 mL falcon tube. After centrifugation at 800 rpm for 5 min, the supernatant was removed and cells were resuspended in 3 mL of cold PBS. This step was repeated twice to wash the cells. The cell pellet from the last washing step was resuspended in 1 mL PBS and filtered through a cell strainer with a pore size of 70 µm for flow cytometry analysis. Gating was chosen depending on an area of forward to side scatter (FSC-A/SSC-A). The fluorescence signal of 100,000 events was measured. Surface attached NLCs were quenched by addition of Trypan Blue in a final concentration of 0.4% (*m/v*) prior to fluorescence detection. The

percentage of cells with high fluorescence emission that took up the LGR labeled NLCs was determined within the sorted population. Data were analyzed using FlowJo™ v10.8.

2.10.5. Endosomal escape

NLCs were evaluated regarding their endosomal escape properties as described previously using hemolysis assay, which represents an established method for the investigation of the endosomal escape [20]. Erythrocytes concentrate was a donation from Tirol Kliniken GmbH (Innsbruck, Austria). In brief, erythrocytes concentrate was diluted 1:100 with sterile HBS pH 7.4. blank NLCs, uncoated R9SA-NLCs, coated PP-R9SA-NLCs, and PP-R9SA-NLCs containing 1 U/mL IAP in a volume of 200 µL were mixed with 200 µL of diluted erythrocytes to obtain final concentrations of 0.1%, 0.05% and 0.01% (*m/v*), respectively. After incubation in a thermomixer at 300 rpm and 37 °C for 4 h, samples were centrifuged at 500 g for 10 min. The absorption of hemoglobin released from the erythrocytes, was measured photometrically at 415 nm. Triton-X at a final concentration of 0.1% (*m/v*) in HBS mixed with diluted erythrocytes was used as the positive control. HBS mixed with erythrocytes served as the negative control.

2.11. Statistical data analysis

Statistical data analysis was performed using GraphPad Prism 5.01. To compare the means of more than two groups one-way ANOVA with Bonferroni post-test was conducted. Repeated measurements at multiple time points were analyzed by two-way ANOVA with Bonferroni post-test. The minimum level of significance was defined as $p < 0.05$.

3. Results and discussion

3.1. Synthesis and characterization of R9SA

Peptide coupling was performed by standard solid phase synthesis on a 2-chlorotritylchloride resin (2-CTC). As displayed in Fig. 1, R9SA was prepared by treating the corresponding peptide resin with stearic acid and *N,N*-diisopropylcarbodiimide (DIC) as coupling reagent in the presence of 1-hydroxybenzotriazol (HOBT) followed by deprotection with trifluoroacetic acid (TFA). As shown in Figure S1, R9SA was synthesized *via* amide bond formation between the N-terminal amino group of nona-L-arginine and the carboxy group of stearic acid. The final product was purified by preparative HPLC and characterized by HPLC and matrix-assisted laser desorption/ionization time-of-flight mass spectrometry (MALDI-TOFMS). R9SA was received with a purity of > 98% determined by HPLC with UV detection at λ = 220 nm, as displayed in Figure S1B. The MALDI-TOF MS analysis of the educt nona-L-arginine and the purified product R9SA are shown in Figure S2. The measured *m/z* ratio for R9SA was 1689.10 Da, which is consistent with the calculated mass of 1689.18 Da. The mass of the purchased nona-L-arginine was confirmed by mass spectrometry showing an *m/z* ratio of 1423.08 (calcd.: *m/z*: 1423.9 $[M+H]^+$) and 1463.10 $[M+K]^+$.

3.2. Characterization of NLCs

NLCs were prepared by solvent diffusion method and, in case of blank NLCs, additionally with a sonicator to obtain nanocarriers of comparable size. The size of NLCs can influence cellular uptake,

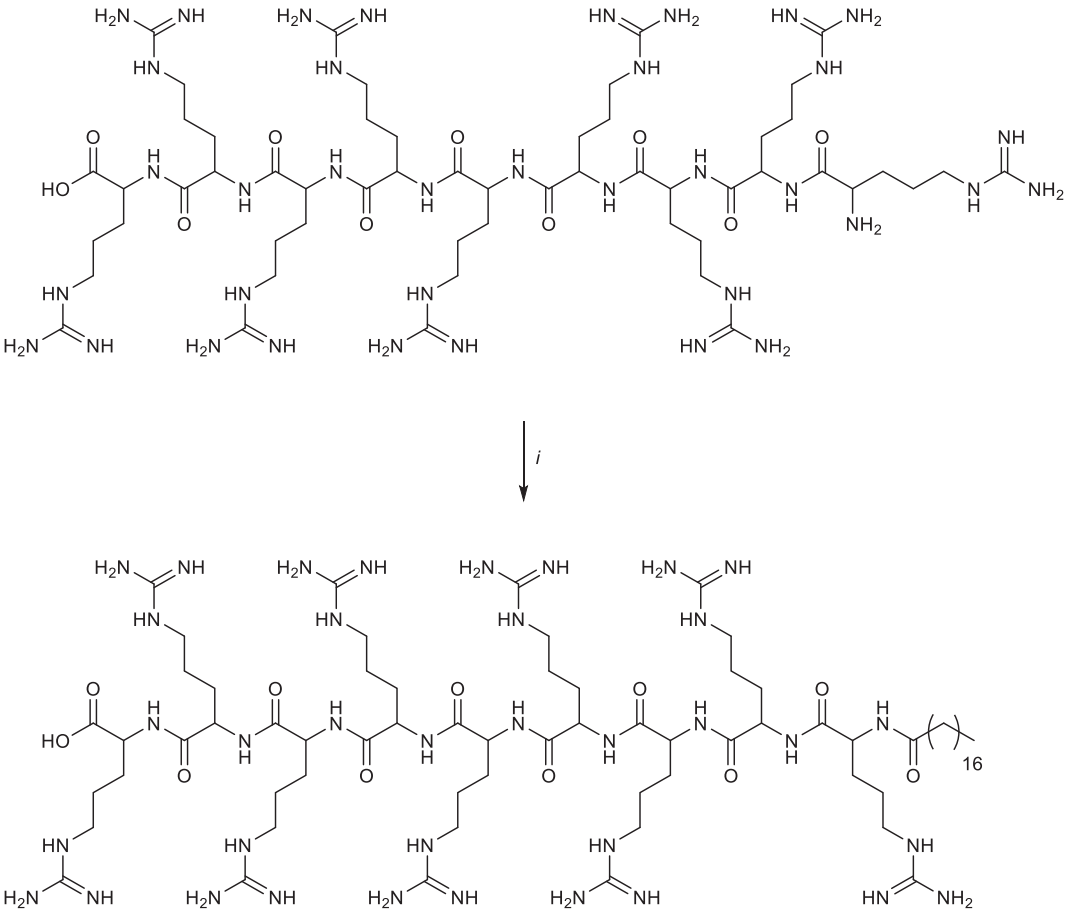

Fig. 1. Synthesis of R9SA: Reagents and conditions: (i) 2-CTC resin, DIC/HOBT, DIPEA, rt, 24 h, TFA/DCM, 98%.

with uptake increasing with decreasing size of NLCs [22,23]. As indicated in Fig. 2, nanocarriers exhibited a comparable size ranging from 146 nm to 152 nm and polydispersity index of 0.2. Only PP-R9SA-NLCs showed a significant increase in size and PDI after 4 h of incubation with IAP. Size and PDI of PP-R9SA-NLCs were 1.8- and 1.9-fold higher after enzymatic cleavage of the phosphate coating, respectively. This observation was also described by Bao Le-Vinh *et al.*, who showed an increase in the size of SLNs over time during incubation with IAP [24]. The increase in mean size could be explained by the relatively slow conversion from negative to positive charge causing aggregation of some NLCs when the zeta potential is during this charge conversion process temporarily not high enough to repulse nanocarriers from each other. Furthermore, during the conversion process the aggregation of anionically and already cationically charged nanocarriers that might be available simultaneously seems plausible.

The zeta potential of NLCs is depicted in Fig. 3. Surface decoration of blank NLCs with R9SA led to a shift in potential from −23.0 mV to 43.2 mV, confirming that nona-L-arginine residues cover the surface of nanocarriers. The highly positive zeta potential compared to previously published data can be explained by the design of PEG-free formulations [25]. Friedl *et al.* demonstrated the shielding effect of PEG surfactants which are currently used in almost all lipid-based nanocarriers due to their high emulsifying properties [20]. The so-called PEG corona masks the positive charges of nanocarriers causing a lower zeta potential and less cellular uptake due to reduced interactions between carrier and cell. Therefore, PEG-free formulations are an attractive alternative to overcome this obstacle. The highest shift in zeta potential was obtained by the polyphosphate coated R9SA-NLCs, leading to NLCs with a zeta potential of −41.8 mV. The longer polyphosphate chains seem to mask not just entirely the shorter nona-L-arginine chains but to introduce additional anionic charges on the surface of the nanocarriers.

3.3. Characterization of saquinavir loaded NLCs

Blank NLCs and R9SA-NLCs were prepared with 3%, 6% and 9% (*m/v*) SQV solution in the lipid phase, respectively. The results of nanocarrier characterization are shown in Table 1. Loading of blank NLCs with SQV did not result in stable NLCs, as the size and PDI of

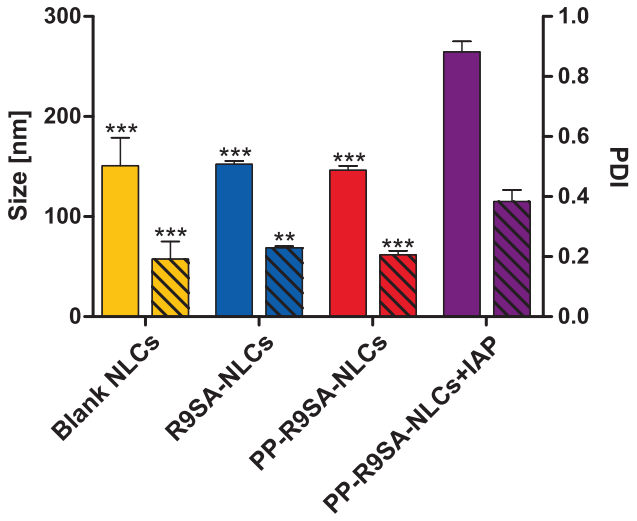

Fig. 2. Size (filled bars) and polydispersity index (lined bars) of 0.01% (*m/v*) blank NLCs, R9SA-NLCs, phosphate coated PP-R9SA-NLCs and PP-R9SA-NLCs after 4 h incubation with 1U/mL of IAP determined by photon correlation spectroscopy. Data are means of three experiments ± standard deviation. ** $p < 0.01$; *** $p < 0.001$ compared with size and PDI of PP-R9SA-NLCs + IAP.

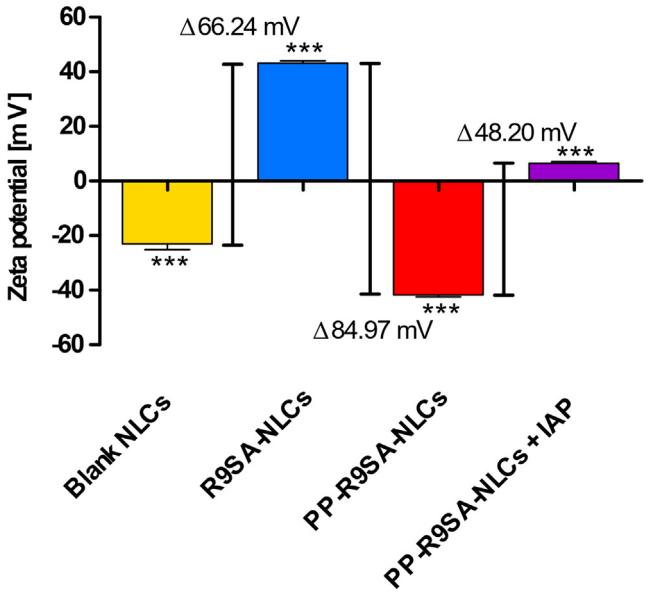

Fig. 3. Zeta potential of 0.01% (*m/v*) NLCs. Charge conversion of phosphate coated NLCs (PP-R9SA-NLCs) after 4 h incubation with 1 U/mL IAP. Data are means of three experiments ± standard deviation. *** $p < 0.001$ compared with each bar.

the nanocarriers increased with increasing amounts of SQV. At an SQV concentration of 9% (*m/v*), blank NLCs were not stable and too polydisperse for a proper determination by DLS. In contrast, R9SA-NLCs showed a small consistent size and low PDI as well as a high positive zeta potential, that was not deviating from R9SA-NLCs without SQV. The nanocarriers with 9% (*m/v*) SQV showed the highest drug loading, as more SQV is available in the lipid solution and can be encapsulated by the nanocarriers. According to the increased drug loading with increasing SQV concentration in the lipid solution, the capacity limit of the NLCs was not reached. In contrast, R9SA-NLCs prepared with a 3% (*m/v*) SQV in lipid solution exhibited the highest encapsulation efficiency. A reason for the decreasing encapsulation efficiency with increasing SQV concentration in the lipid solution could be the low water solubility of SQV and the competition of increasing amounts of SQV for the limited space in the lipid core of NLCs. This observation is consistent with other studies where SQV was also encapsulated in lipid based nanocarriers in increasing amounts [26]. Yuan et al. demonstrated that the encapsulation efficiency of NLCs mainly depends on the quantity of available liquid lipids [27]. Increasing the concentration of liquid lipids in R9SA-NLCs could therefore improve the encapsulation efficiency of SQV.

3.4. Stability in simulated biorelevant fluids

The stability of blank NLCs, R9SA-NLCs and PP-R9SA-NLCs was investigated in different simulated biorelevant fluids before and after an incubation for 4 h. As indicated in Fig. 4, all formulations were stable in FaSSIF after preparation except R9SA-NLCs. The positive charges of R9SA-NLCs might be masked by the negatively charged bile salts and phospholipids in FaSSIF [21]. These ionic interactions result in a condensation of the charge at the electric double layer on the nanocarrier surface and less electrostatic repulsion between NLCs causing their aggregation [29]. In contrast, the polyphosphate coating provided an effective protection for the nanocarriers, which was repealed by the addition of IAP. The positively charged R9SA-NLCs showed agglomeration in SIF as also observed in FaSSIF since the high phosphate concentration of the buffer reduced the electrostatic repulsion of NLCs. In particular, pancreatin increased the size of blank NLCs after 4 h. Since the sur-

Table 1
Characterization of blank NLCs and R9SA-NLCs regarding size, PDI, zeta potential, drug load and encapsulation efficiency. Data are means of three experiments ± standard deviation.

Formulation	SQV [% of lipid phase m/v]	Size [nm]	PDI	Zeta potential [mV]	Drug load [µg/mg]	Encapsulation efficiency [%]
Blank NLCs	3	1191.0 ± 125.0	0.23 ± 0.15	8.0 ± 7.4	/	/
	6	2580.7 ± 577.8	0.60 ± 0.25	5.1 ± 0.6	/	/
	9	Not measurable	Not measurable	Not measurable	/	/
R9SA-NLCs	3	162.7 ± 8.1	0.17 ± 0.02	44.0 ± 1.8	23.5 ± 3.3	80.6 ± 11.2
	6	162.2 ± 23.3	0.17 ± 0.02	44.5 ± 0.7	36.6 ± 9.2	64.7 ± 16.2
	9	169.4 ± 5.8	0.19 ± 0.01	45.3 ± 0.8	46.5 ± 12.5	60.0 ± 15.1

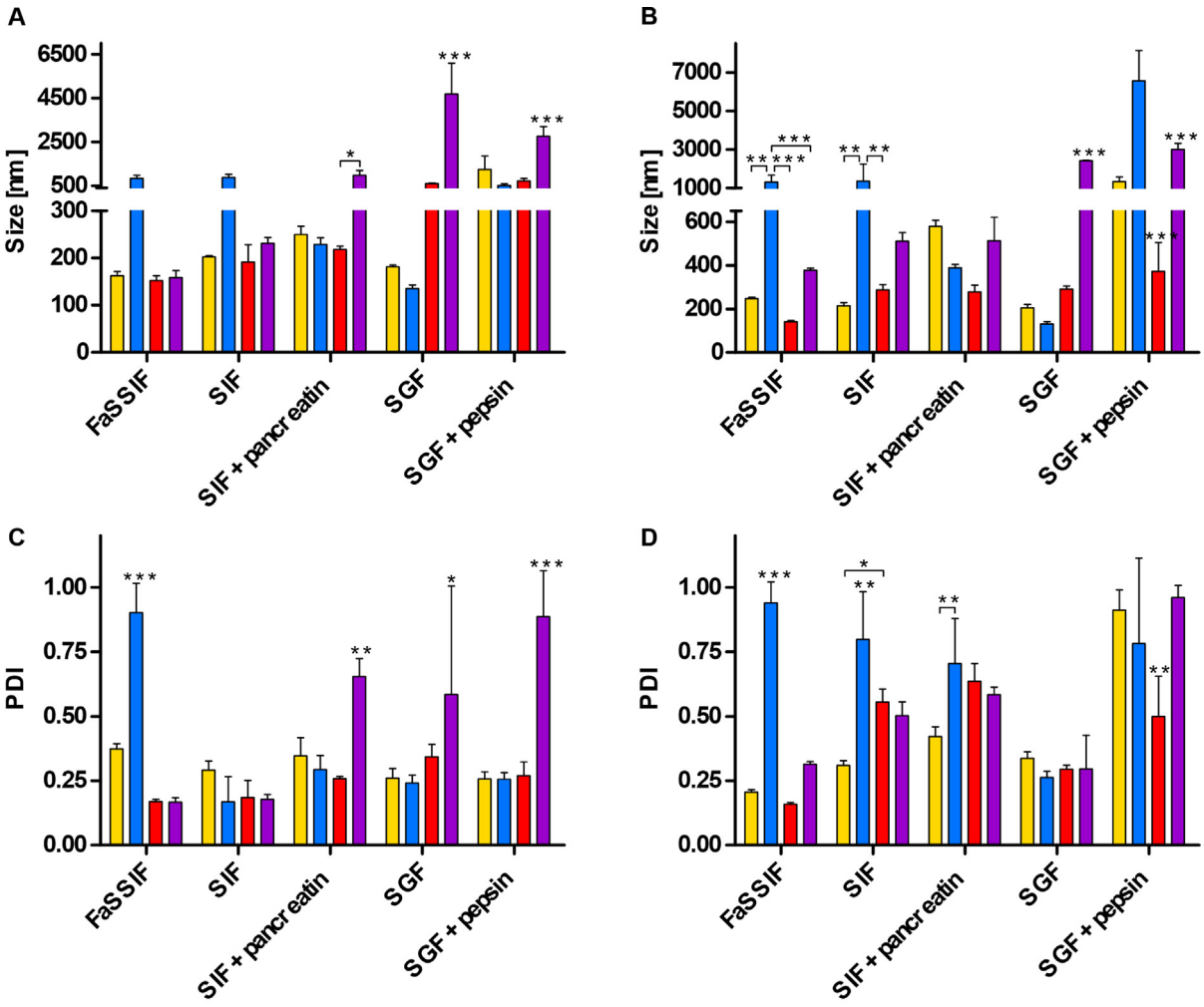

Fig. 4. Stability of blank NLCs (orange), R9SA-NLCs (blue), PP-R9SA-NLCs (red) and PP-R9SA-NLCs containing 1 U/mL IAP (purple) in FaSSIF, SIF, SIF containing pancreatin, SGF, and SGF containing pepsin. Size of nanocarriers was determined immediately after dilution with buffer (A) and after 4 h (B) of incubation at 37 °C. Equally, the PDI was measured immediately (C) and after 4 h (D). Indicated data are means of three experiments ± standard deviation. * $p < 0.05$; ** $p < 0.01$; *** $p < 0.001$ compared with all other bars or with indicated other bars. (For interpretation of the references to colour in this figure legend, the reader is referred to the web version of this article.)

face of blank NLCs is only covered with phospholipids, enzymes can easily lipolyze the phospholipids limiting their stability [30]. PP-R9SA-NLCs showed a slight increase in size by SIF containing pancreatin, indicating only a minor effect of pancreatin. SGF caused an increase in size of PP-R9SA-NLCs. One reason for this might be the acidic pH, leading to protonation of the two slightly acidic phosphates at the polyphosphate termini [31]. These protonated and uncharged polyphosphates on the surface of NLCs decrease the electrostatic repulsion inducing their aggregation. Incubation of the nanocarriers in SGF containing pepsin resulted in an increased size and PDI for all different NLCs. Therefore, NLCs are not stable in this medium and need to be enteric-coated for efficient drug delivery. In case of PP-R9SA-NLCs, the size increase after 4 h was significantly lower compared to other nanocarriers. An explanation for this observation might be a higher resistance of these nanocarriers towards an enzymatic degradation because of the polyphosphate coating.

3.5. Phosphate release and charge conversion

The phosphate coating of charge-converting nanocarriers can be obtained in two ways. On the one hand nanocarriers containing phosphorylated surfactants or polymers can be utilized [28]. On the other hand positively charged nanocarriers can be coated with

polyphosphates [24]. In this study, the latter concept was applied to form polyphosphate-coated PP-R9SA-NLCs. The obtained nanocarriers were investigated for phosphate release after cleaving the polyphosphate chains into monophosphates by intestinal alkaline phosphatase. The time dependent phosphate release from PP-R9SA-NLCs and PP-R9SA-NLCs incubated with IAP is displayed in Fig. 5. When incubated with IAP, more than half of the polyphosphate was cleaved within the first 15 min. After 60 min, more than 80% polyphosphate was cleaved by the enzyme. PP-R9SA-NLCs incubated without IAP showed a negligible amount of released monophosphates over this time-period. As shown in Fig. 3, cleavage of the polyphosphate chains led to a degradation of the polyphosphate coating resulting in a charge conversion from −41.8 to 6.4 mV as the positively charged nona-L-arginine was exposed again on the surface. Since cleaved free phosphate can still accumulate and interact with the positive arginine residues, a zeta potential shift back to the original surface charge of uncoated R9SA does not seem to be feasible. This observation is in agreement with findings of Le *et al.* who demonstrated a charge conversion from −14.1 mV to 4.2 mV, without regaining the original zeta potential of uncoated nanocarriers [14].

3.6. Mucus diffusion study

The ability of NLCs to penetrate into mucus was investigated *via* the rotating tube method. As displayed in Fig. 6, R9SA-NLCs showed the lowest diffusivity. This can be explained by the cationic charges of the arginine groups causing strong ionic interactions with the negatively charged mucus. Sialic and sulfate moieties of mucin glycoproteins likely interact with the positively charged guanidine groups of R9SA-NLCs [45]. Nanocarriers that get stuck inside the mucus cannot reach the underlying epithelial cells essentially limiting their efficacy. These interactions with mucus can be avoided by a polyphosphate coating masking the positive charges of polyarginine on the surface of nanocarriers. PP-R9SA-NLCs showed significantly higher permeability into deeper mucus segments that was in the third segment even 3.2- and 4.7-fold higher than blank NLCs and R9SA-NLCs, respectively. Blank NLCs indicated higher diffusivity than R9SA-NLCs but lower than PP-R9SA-NLCs that could be explained by the zwitterionic surface. The interactions between the zwitterionic surface and the negatively charged mucus are less intense, resulting in higher penetration into the mucus than positively charged NLCs.

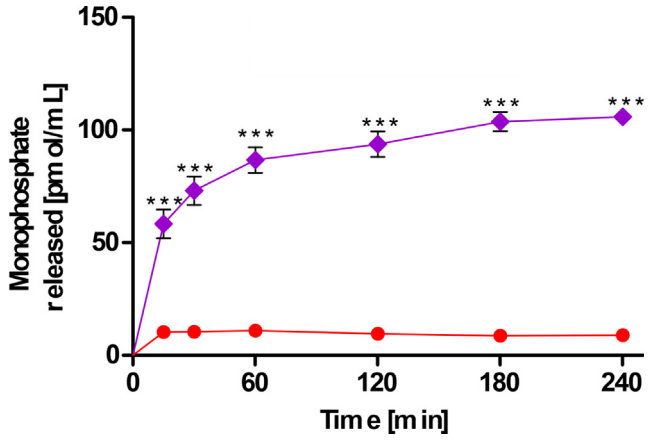

Fig. 5. Time-dependent phosphate release during incubation of PP-R9SA-NLCs with (purple) and without (red) 1 U/mL IAP. Data are means of three experiments ± standard deviation. *** $p < 0.001$ compared with PP-R9SA-NLCs without IAP. (For interpretation of the references to colour in this figure legend, the reader is referred to the web version of this article.)

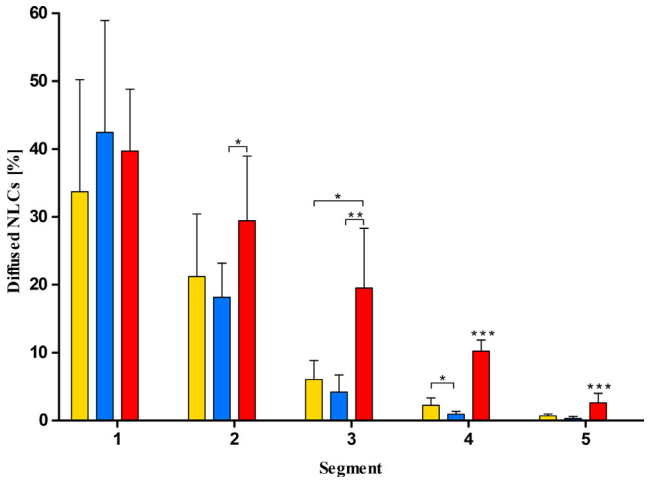

Fig. 6. Mucus diffusion in percentage of LGR labeled blank NLCs (orange), R9SA-NLCs (blue) and PP-R9SA-NLCs (red) after 24 h rotation at 50 rpm and 37 °C. Indicated values are means of three experiments ± standard deviation. * $p < 0.05$; ** $p < 0.01$ and *** $p < 0.001$ compared with all other bars (PP-R9SA-NLCs) of the same segment and with indicated other bars. (For interpretation of the references to colour in this figure legend, the reader is referred to the web version of this article.)

3.7. Cytotoxicity

Blank NLCs, R9SA-NLCs and PP-R9SA-NLCs were evaluated regarding cytotoxic effects on Caco-2 cells in concentrations of 0.1%, 0.05%, and 0.01% (*m/v*) by resazurin assay. Since only living cells can reduce resazurin to the highly fluorescent resorufin, a high measured fluorescence intensity correlates with high cell viability. As displayed in Fig. 7, after 4 h of incubation viability of cells was almost 100% for all nanocarriers with no significant differences. Even after 24 h, the viability of cells decreased only slightly to about 95% for all NLCs at a concentration of 0.1% (*m/v*). Since all formulations in the three different concentrations show a higher viability than 90%, it can be assumed that the NLCs have negligible cytotoxic effects. Therefore, the nanocarriers in the evaluated concentrations could be used for further cell studies. The results are consistent with those of Futaki *et al.*, who demonstrated the cytocompatibility of stearyl-polyarginine, which will have the greatest influence on cell viability of all components used in NLCs [32].

3.8. Phosphate cleavage by Caco-2 cells

Caco-2 cells are known to express the brush border enzyme alkaline phosphatase [33]. According to the findings of Matsumoto *et al.*, phosphatase activity increases linearly after cells have reached a confluent monolayer [34]. Therefore, the cultivation time of cells was set at 12 days to ensure confluent monolayer and sufficient alkaline phosphatase activity. PP-R9SA-NLCs were applied to cells in a concentration of 0.01% (*m/v*) with and without the addition of PIC2 for 4 h. The results of time dependent phosphate cleavage are depicted in Fig. 8. After 30 min, the cleavage of polyphosphate by Caco-2 cells was significantly higher for NLCs incubated without PIC2. By the end of the incubation time, PP-R9SA-NLCs showed a 2.7-fold higher phosphate release than the nanocarriers in the presence of PIC2. The release of monophosphate indicates the cleavage of polyphosphates by cell membrane bound phosphatase causing a charge conversion of the nanocarriers. This conversion restores the positively charged surface required for enhanced internalization of NLCs into cells. Since the phosphate release was still increasing linearly after 4 h, not all of the polyphosphate had been cleaved within the incubation period. Even in the presence of PIC2 phosphate is still released from NLCs,

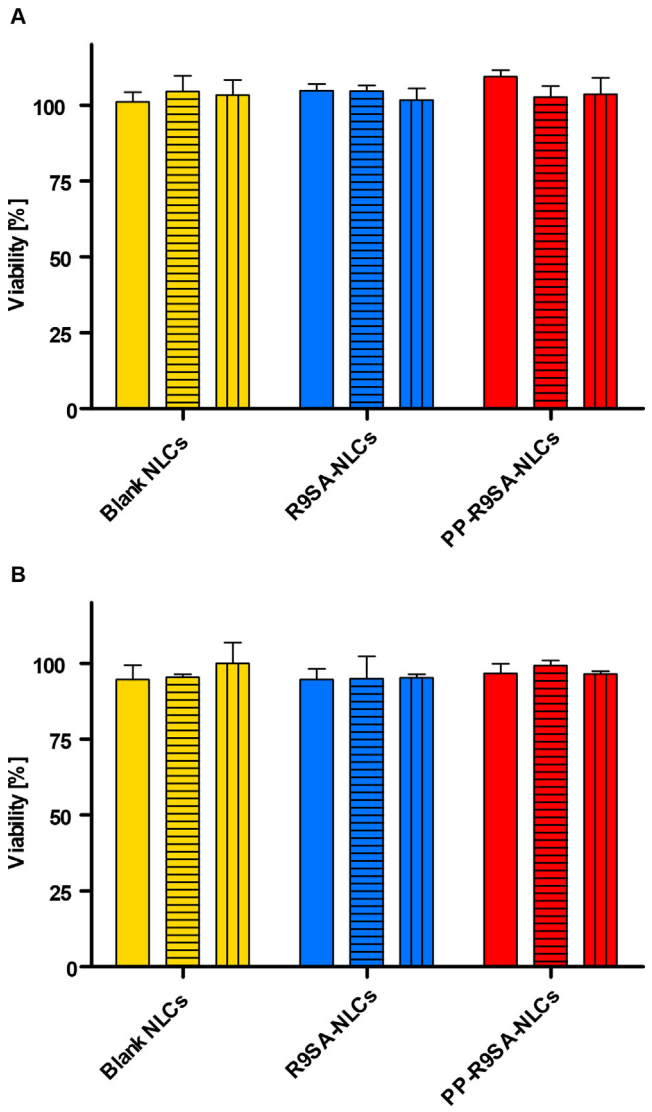

Fig. 7. Viability of Caco-2 cells after treatment with 0.1% (filled bars), 0.05% (horizontal lined bars) and 0.01% (*m*/*v*) (vertical lined bars) NLCs for 4 h (A) and 24 h (B). 0.1% (*m*/*v*) Triton X 100 served as negative control. Data are means of three experiments ± standard deviation.

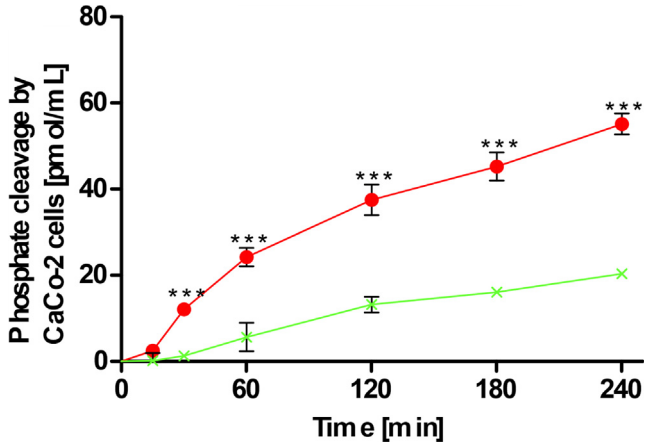

Fig. 8. Time-dependent phosphate release during incubation of 0.01% (*m*/*v*) PP-R9SA-NLCs (red) on Caco-2 cells. Phosphatase inhibitor cocktail added to PP-R9SA-NLCs in a final concentration at 1% (*v*/*v*) served as control (green). Data are means of three experiments ± standard deviation. *** $p < 0.001$ compared with PP-R9SA-NLCs with addition of PIC 2. (For interpretation of the references to colour in this figure legend, the reader is referred to the web version of this article.)

indicating that not all phosphatases were inhibited by PIC2. This observation is in agreement with results having been obtained in similar studies, showing an incomplete inhibition of phosphatase [17].

3.9. In vitro cellular uptake studies

The cell-penetrating peptide arginine is known for its properties to enhance cellular uptake of proteins [35], as it can be taken up not only by endocytosis but also *via* translocation through the cell membrane [36]. Unlike other CPPs such as lysine, arginine provides this effect regardless of pH because the guanidinium head group is positively charged at all physiological pH values [37]. To investigate whether this effect can be transferred to NLCs, the cellular uptake of R9SA-decorated nanocarriers in Caco-2 cells was studied. Cell uptake of LGR labeled nanocarriers is illustrated in Fig. 9A.

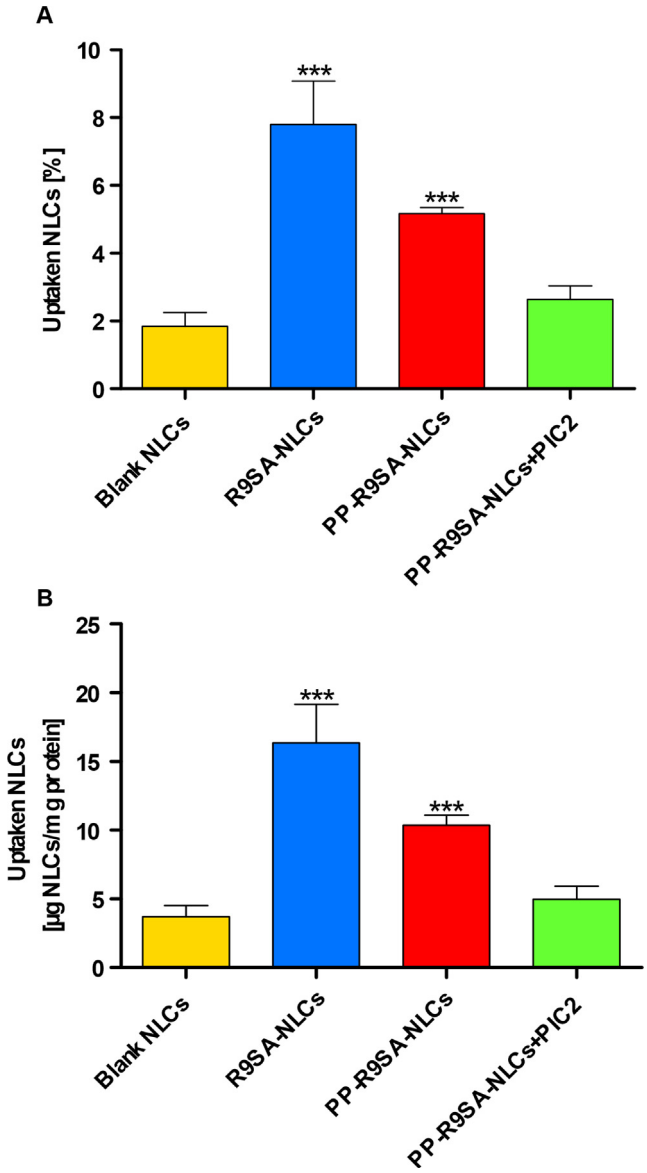

Fig. 9. *In vitro* cellular uptake of Lumogen red labeled NLCs. (A) Cellular uptake calculated in percentage compared with 100%. (B) Cellular uptake determined in relation to protein content. Shown data are means of three experiments ± standard deviation. *** $p < 0.001$ compared with all other bars. (For interpretation of the references to colour in this figure legend, the reader is referred to the web version of this article.)

NLCs with polyarginine chains on the surface showed the highest internalization by cells compared to the blank NLCs after 3 h of incubation. Cellular uptake of R9SA-NLCs and PP-R9SA-NLCs was increased 5.2-fold and 3.1-fold, respectively, compared to the blank NLCs. One reason for this may be the polycations of the surfactant, which exhibit charge-mediated interactions with the cells [38]. The polyphosphate coating of the PP-R9SA-NLCs lowered the uptake efficiency compared to the uncoated carriers, showing the highest values with 16.37 µg/mg protein. Since the coating needs to be cleaved by IAP before uptake to unleash the cell-penetrating properties of polyarginine on the nanocarrier surface, the results of PP-R9SA-NLCs are significantly lower than those of R9SA-NLCs. Cleavage depends on phosphatases' availability, which increases with the cultivation time after the confluence of cells [33]. Therefore, the cleavage and hence the uptake of PP-R9SA-NLCs could be higher if the study was conducted after a longer growth period of the cells. This is even more evident when PIC2 is added to the NLCs, resulting in less cleavage of phosphate and thus even less uptake of NLCs. PP-R9SA-NLCs showed 2.2-fold enhanced cell uptake compared to PP-R9SA-NLCs when incubated with PIC2. Since the cell density in each well can vary, cell uptake was normalized to the protein density in the corresponding well. Fig. 9B shows that the seeding and growth of cells were consistent, as the results were comparable to data without taking protein density into account.

Cellular uptake was examined by flow cytometer analysis after three hours of incubation of the nanocarriers on Caco-2 cells, followed by trypsinization of cells for FACS. The gating performed selected the main population that contained only viable and single Caco-2 cells and excluded fragmented cells. As displayed in Fig. 10, uptake of administered nanocarriers resulted in a shift in fluorescence intensity, which was increased in the following rank order: HBS < blank NLCs < PP-R9SA-NLCs + PIC2 < PP-R9SA-NLCs < R9SA-NLCs. This observation is in accordance with results shown in Fig. 11A, demonstrating a significantly increased cellular uptake for R9SA-NLCs in comparison to blank NLCs and PP-R9SA-NLCs + PIC2. The formulations R9SA-NLCs and PP-R9SA-NLCs were internalized by 64.0% and 50.3% of Caco-2 cells, respectively, reaching a 6.7- and 5.3-fold enhancement compared to blank NLCs.

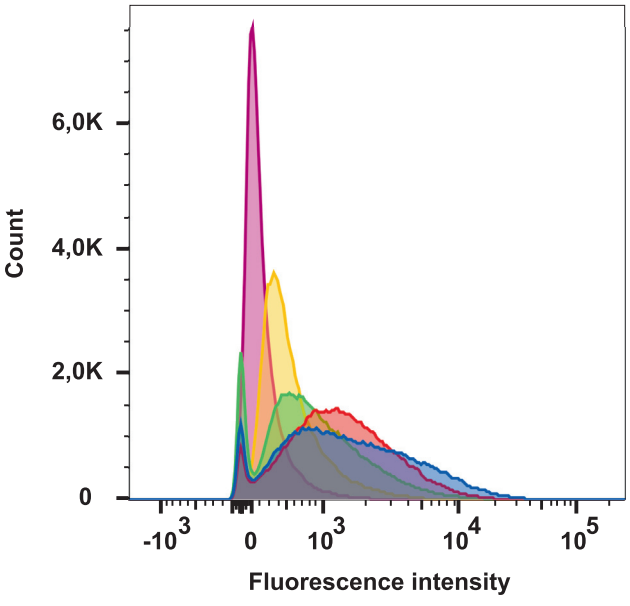

Fig. 10. Fluorescence intensity shift after cell uptake of Lumogen red loaded 0.01% (*m*/*v*) blank NLCs (orange), R9SA-NLCs (blue), PP-R9SA-NLCs (red), PP-R9SA-NLCs + PIC2 (green) and HBS (purple) as control detected by flow cytometer. The data shown is a replication of three experiments. (For interpretation of the references to colour in this figure legend, the reader is referred to the web version of this article.)

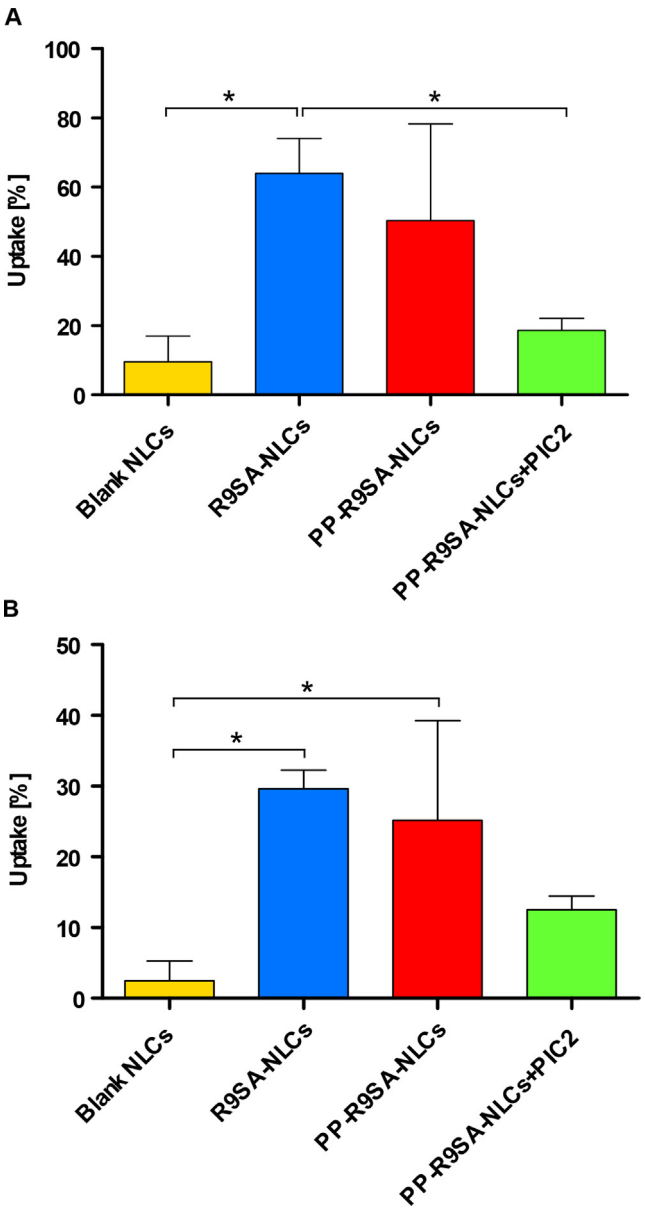

Fig. 11. Percentage of cells showing a fluorescence signal after cellular uptake of Lumogen red labeled blank NLCs, R9SA-NLCs, PP-R9SA-NLCs and PP-R9SA-NLCs + PIC2. Nanocarriers were incubated on cells at a concentration of 0.01% (*m*/*v*) for 3 h without (A) and with (B) Trypan Blue quenching of surface absorbed NLCs. Indicated data are means of three experiments ± standard deviation. * $p < 0.05$. (For interpretation of the references to colour in this figure legend, the reader is referred to the web version of this article.)

Fig. 11B shows the cellular uptake after quenching the surface absorbed nanocarriers by adding Trypan Blue to the cell suspension [39]. Uptake of R9SA-NLCs was ~2-fold higher before quenching, indicating that about 50% of nanocarriers were only adsorbed on the surface of cells and not fully internalized. For blank NLCs, this effect was even more pronounced, showing 4.9-fold higher uptake before quenching. The uptake of R9SA-NLCs and PP-R9SA-NLCs was 15.6- and 13.2-fold higher than that of blank NLCs, respectively. This proves that the cellular uptake of NLCs can be significantly increased by the modification with a CPP in the form of a surfactant. The impact of charge conversion before cellular

uptake was confirmed by the 2.0-fold enhanced uptake of PP-R9SA-NLCs compared to NLCs in the presence of the phosphatase inhibitor cocktail 2.

3.10. Endosomal escape

Studies of the interaction between red blood cells and nanocarriers can help to predict whether a nanocarrier is able to exit the endosomal pathway or not [40]. Nanocarriers taken up *via* the endocytic pathway are encapsulated in endosomes and are subsequently degraded in lysosomes, leading to a complete loss of the drug delivery system [41]. To address this issue, endosomal escape of nanocarriers must be ensured. Nanocarriers that interact more with the cell membrane are supposed to be capable of lysing the endosomes, resulting in an endosomal escape. In the hemolysis assay, high interaction and suitable properties for endosomal escape can be observed for nanocarriers that show a high percentage of hemolysis. As displayed in Fig. 12, R9SA-NLCs showed the highest hemolysis values at all concentrations. Even at the lowest concentration, 84.2% of erythrocytes were lysed. This observation can be attributed to the CPP R9SA on NLCs, as the positive guanidinium headgroups interact with negatively charged polysaccharides on the cell membrane causing destabilization of the membrane [42]. This observation is consistent with results of other studies indicating a high endosomal escape capacity of oligoarginines in early endosomes [43]. Blank NLCs exhibited less hemolysis than the R9SA-NLCs but higher values than the PP-R9SA-NLCs. The similar composition of the NLCs surface compared to the cell membrane could be a reason for the higher values, as the nanocarrier layer consists of phospholipids. The lowest interaction between red blood cells and nanocarriers was observed for PP-R9SA-NLCs, showing 35.7% hemolysis at 0.1% (*m/v*) and 0.1% hemolysis at 0.01% (*m/v*) NLCs. Therefore, the polyphosphate coating resulted in less cell interaction and less lysis of erythrocytes. Since mammalian erythrocytes cannot express alkaline phosphatase [44], PP-R9SA-NLCs containing IAP were used to investigate whether cleavage of the phosphate coating impacted interaction with cells. The addition of IAP resulted in a significant increase in lysed erythrocytes at all concentrations compared with PP-R9SA-NLCs without IAP. Since cleavage of polyphosphate depends on the time and concentration of enzyme, differences were more pronounced in samples with lower concentrations. The hemolysis of PP-R9SA-NLCs with IAP at a concentration of 0.01% (*m/v*) was 76.6-fold higher than without IAP. This observation may be a proof of concept, as cleavage of polyphosphate uncoats the positively charged polyarginine residues on the surface of the NLCs that can interact with the cell membrane for endosomal escape.

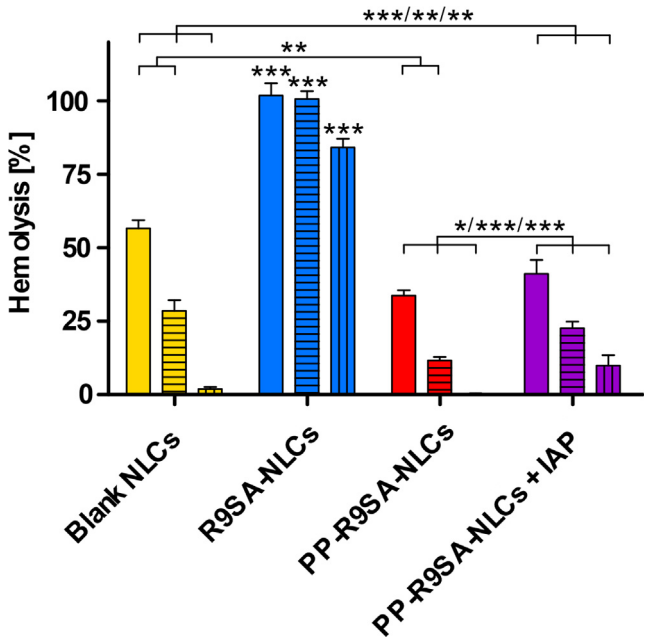

Fig. 12. Hemolysis of erythrocytes concentrate after incubation with nanocarriers in final concentrations at 0.1% (filled bars), 0.05% (horizontal lined bars) and 0.01% (*m/v*) (vertical lined bars) for 4 h. Displayed values are means of three experiments ± standard deviation. * $p < 0.05$; ** $p < 0.01$; *** $p < 0.001$ compared with all other bars (R9SA-NLCs) and with indicated other bars.

4. Conclusion

The design of nanocarriers providing on the one hand high mucus permeating properties and on the other hand also sufficient cellular uptake is one of the major obstacles that needs to be mastered in mucosal drug delivery. As high mucus permeation is mainly provided by negatively charged nanocarriers, that show just poor cellular uptake, charge converting systems seem to be the key to address this dilemma. Therefore, NLCs were decorated with the polycationic cell-penetrating peptide R9SA providing a positive surface charge that was converted to negative by the additional coating with PP. Saquinavir as BCS class IV model drug was incorporated in these nanocarriers. When PP-R9SA-NLCs were incubated with intestinal alkaline phosphatase and on Caco-2 cells, time dependent cleavage of the polyphosphate was shown, uncoating the polycationic R9SA on the nanocarrier surface. These observations are consistent with previous studies [11] indicating an efficient polyphosphate cleavage by the enzyme causing a charge conversion of Δ48.2 mV from negative to positive zeta potential. This charge conversion was the highest measured shift described in the literature so far [10,14,46]. Furthermore, NLCs showed no cytotoxicity over 24 h. PP-R9SA-NLCs exhibited significantly higher mucus permeating properties than R9SA-NLCs but still high cellular uptake by Caco-2 cells due to charge conversion on the cellular membrane. Enhanced cellular interactions were also observed with red blood cells suggesting that these nanocarriers can escape endosomes under simulated physiological conditions. The high potential of these nanocarriers was demonstrated by their mucus permeating properties and a pronounced cellular uptake. The concept of this study can be transferred to various other types of nanocarriers and might pave the way to a new generation of nanocarriers for mucosal drug delivery.

CRediT authorship contribution statement

Patrick Knoll: Conceptualization, Methodology, Investigation, Visualization, Writing – original draft, Writing – review & editing. **Nikolas Hörmann:** Methodology, Investigation, Visualization, Writing – original draft, Writing – review & editing. **Nguyet-Minh Nguyen Le:** Methodology, Investigation. **Richard Wibel:** Methodology, Visualization. **Ronald Gust:** Writing – review & editing, Supervision. **Andreas Bernkop-Schnürch:** Conceptualization, Writing – review & editing, Funding acquisition, Supervision.

Declaration of Competing Interest

The authors declare that they have no known competing financial interests or personal relationships that could have appeared to influence the work reported in this paper.

Acknowledgment

The authors would like to thank Anton Amadeus Hörmann (Department of Nuclear Medicine, Medical University of Innsbruck, 6020 Innsbruck, Austria) for providing the reaction vessels and apparatus and for his kind assistance with the analysis of the final products. This work was supported by a doctoral scholarship for promotion of young researchers at the Leopold-Franzens-University Innsbruck.

Appendix A. Supplementary data

Supplementary data to this article can be found online at https://doi.org/10.1016/j.jcis.2022.07.160.

References

[1] S. Khan, S. Baboota, J. Ali, S. Khan, R.S. Narang, J.K. Narang, Nanostructured lipid carriers : An emerging platform for improving oral bioavailability of lipophilic drugs, (2015). https://doi.org/10.4103/2230-973X.167661.
[2] B.J. Boyd, C.A.S. Bergström, Z. Vinarov, M. Kuentz, J. Brouwers, P. Augustijns, M. Brandl, A. Bernkop-Schnürch, N. Shrestha, V. Préat, A. Müllertz, A. Bauer-Brandl, V. Jannin, Successful oral delivery of poorly water-soluble drugs both depends on the intraluminal behavior of drugs and of appropriate advanced drug delivery systems, Eur. J. Pharm. Sci. 137 (2019) 104967, https://doi.org/10.1016/j.ejps.2019.104967.
[3] A.B. Kovačević, R.H. Müller, C.M. Keck, Formulation development of lipid nanoparticles: Improved lipid screening and development of tacrolimus loaded nanostructured lipid carriers (NLC), Int. J. Pharm. 576 (2020) 118918, https://doi.org/10.1016/j.ijpharm.2019.118918.
[4] E.J.A. Suys, D.H.S. Brundel, D.K. Chalmers, C.W. Pouton, C.J.H. Porter, Interaction with biliary and pancreatic fluids drives supersaturation and drug absorption from lipid-based formulations of low (saquinavir) and high (fenofibrate) permeability poorly soluble drugs, J. Control. Release. 331 (2021) 45–61, https://doi.org/10.1016/j.jconrel.2021.01.007.
[5] B. Homayun, X. Lin, H.-J. Choi, Challenges and recent progress in oral drug delivery systems for biopharmaceuticals, Pharmaceutics. 11 (3) (2019) 129.
[6] M. Boegh, C. Foged, A. Müllertz, H. Mørck Nielsen, Mucosal drug delivery: Barriers, in vitro models and formulation strategies, J. Drug Deliv. Sci. Technol. 23 (2013) 383–391, https://doi.org/10.1016/S1773-2247(13)50055-4.
[7] A. Bernkop-Schnürch, Strategies to overcome the polycation dilemma in drug delivery, Adv. Drug Deliv. Rev. 136–137 (2018) 62–72, https://doi.org/10.1016/j.addr.2018.07.017.
[8] P. Stenberg, H. Lennernas, Chitosans as absorption enhancers of poorly absorbable drugs 3 : Influence of mucus on absorption enhancement, 8 (1999) 335–343.
[9] I. Nazir, A. Fürst, N. Lupo, A. Hupfauf, R. Gust, A. Bernkop-Schnürch, Zeta potential changing self-emulsifying drug delivery systems: A promising strategy to sequentially overcome mucus and epithelial barrier, Eur. J. Pharm. Biopharm. 144 (2019) 40–49, https://doi.org/10.1016/j.ejpb.2019.09.007.
[10] Z.B. Akkus, I. Nazir, A. Jalil, M. Tribus, A. Bernkop-Schnürch, Zeta Potential Changing Polyphosphate Nanoparticles: A Promising Approach to Overcome the Mucus and Epithelial Barrier, Mol. Pharm. 16 (2019) 2817–2825, https://doi.org/10.1021/acs.molpharmaceut.9b00355.
[11] F. Sharifi, I. Nazir, M.H. Asim, M. Jahangiri, P. Ebrahimnejad, B. Matuszczak, A. Bernkop-Schnürch, Zeta potential changing self-emulsifying drug delivery systems utilizing a novel Janus-headed surfactant: A promising strategy for enhanced mucus permeation, J. Mol. Liq. 291 (2019) 111285.
[12] J.D. Wolf, M. Kurpiers, R.X. Götz, S. Zaichik, A. Hupfauf, D. Baecker, R. Gust, A. Bernkop-Schnürch, Phosphorylated PEG-emulsifier: Powerful tool for development of zeta potential changing self-emulsifying drug delivery systems (SEDDS), Eur. J. Pharm. Biopharm. 150 (2020) 77–86, https://doi.org/10.1016/j.ejpb.2020.03.004.
[13] V.P. Torchilin, H. Benson, I. Toth, Cell penetrating peptide-modified pharmaceutical nanocarriers for intracellular drug and gene delivery, Biopolym. - Pept. Sci. Sect. 90 (5) (2008) 604–610.
[14] N.M.N. Le, C. Steinbring, B. Le-Vinh, A. Jalil, B. Matuszczak, A. Bernkop-Schnürch, Polyphosphate coatings: A promising strategy to overcome the polycation dilemma, J. Colloid Interface Sci. 587 (2021) 279–289, https://doi.org/10.1016/j.jcis.2020.12.019.
[15] J. Xie, Y. Bi, H. Zhang, S. Dong, L. Teng, R.J. Lee, Z. Yang, Cell-Penetrating Peptides in Diagnosis and Treatment of Human Diseases: From Preclinical Research to Clinical Application, Front. Pharmacol. 11 (2020) 1–23, https://doi.org/10.3389/fphar.2020.00697.
[16] F.Q. Hu, S.P. Jiang, Y.Z. Du, H. Yuan, Y.Q. Ye, S. Zeng, Preparation and characteristics of monostearin nanostructured lipid carriers, Int. J. Pharm. 314 (2006) 83–89, https://doi.org/10.1016/j.ijpharm.2006.01.040.
[17] C. Leichner, M. Jelkmann, F. Prüfert, F. Laffleur, A. Bernkop-Schnürch, Intestinal enzyme delivery: Chitosan/tripolyphosphate nanoparticles providing a targeted release behind the mucus gel barrier, Eur. J. Pharm. Biopharm. 144 (2019) 125–131, https://doi.org/10.1016/j.ejpb.2019.09.012.
[18] A. Jalil, M.H. Asim, I. Nazir, B. Matuszczak, A. Bernkop-Schnürch, Self-emulsifying drug delivery systems containing hydrophobic ion pairs of polymyxin B and agaric acid: A decisive strategy for enhanced antimicrobial activity, J. Mol. Liq. 311 (2020) 113298, https://doi.org/10.1016/j.molliq.2020.113298.
[19] Z.B. Akkuş-Dağdeviren, J.D. Wolf, M. Kurpiers, I. Shahzadi, C. Steinbring, A. Bernkop-Schnürch, Charge reversal self-emulsifying drug delivery systems: A comparative study among various phosphorylated surfactants, J. Colloid Interface Sci. 589 (2021) 532–544, https://doi.org/10.1016/j.jcis.2021.01.025.
[20] J.D. Friedl, C. Steinbring, S. Zaichik, N.M.N. Le, A. Bernkop-Schnürch, Cellular uptake of self-emulsifying drug-delivery systems: Polyethylene glycol versus polyglycerol surface, Nanomedicine. 15 (2020) 1829–1841, https://doi.org/10.2217/nnm-2020-0127.
[21] R. Wibel, D.E. Braun, L. Hämmerle, A.M. Jörgensen, P. Knoll, W. Salvenmoser, C. Steinbring, A. Bernkop-Schnürch, In Vitro Investigation of Thiolated Chitosan Derivatives as Mucoadhesive Coating Materials for Solid Lipid Nanoparticles, Biomacromolecules 22 (9) (2021) 3980–3991.
[22] H. Li, M. Chen, Z. Su, M. Sun, Q. Ping, Size-exclusive effect of nanostructured lipid carriers on oral drug delivery, Int. J. Pharm. 511 (2016) 524–537, https://doi.org/10.1016/j.ijpharm.2016.07.049.
[23] H. Mu, R. Holm, Solid lipid nanocarriers in drug delivery: characterization and design, Expert Opin. Drug Deliv. 15 (2018) 771–785, https://doi.org/10.1080/17425247.2018.1504018.
[24] B. Le-Vinh, C. Steinbring, R. Wibel, J.D. Friedl, A. Bernkop-Schnürch, Size shifting of solid lipid nanoparticle system triggered by alkaline phosphatase for site specific mucosal drug delivery, Eur. J. Pharm. Biopharm. 163 (2021) 109–119, https://doi.org/10.1016/j.ejpb.2021.03.012.
[25] M. Sun, Y. Gao, Z. Zhu, H. Wang, C. Han, X. Yang, W. Pan, A systematic in vitro investigation on poly-arginine modified nanostructured lipid carrier: Pharmaceutical characteristics, cellular uptake, mechanisms and cytotoxicity, Asian J. Pharm. Sci. 12 (2017) 51–58, https://doi.org/10.1016/j.ajps.2016.07.007.
[26] Y.C. Kuo, H.F. Ko, Targeting delivery of saquinavir to the brain using 83–14 monoclonal antibody-grafted solid lipid nanoparticles, Biomaterials 34 (2013) 4818–4830, https://doi.org/10.1016/j.biomaterials.2013.03.013.
[27] H. Yuan, L.L. Wang, Y.Z. Du, J. You, F.Q. Hu, S. Zeng, Preparation and characteristics of nanostructured lipid carriers for control-releasing progesterone by melt-emulsification, Colloids Surf. B Biointerfaces 60 (2007) 174–179, https://doi.org/10.1016/j.colsurfb.2007.06.011.
[28] S. Zaichik, C. Steinbring, M. Jelkmann, A. Bernkop-Schnürch, Zeta potential changing nanoemulsions: Impact of PEG-corona on phosphate cleavage, Int. J. Pharm. 581 (2020) 119299, https://doi.org/10.1016/j.ijpharm.2020.119299.
[29] M.O. Fatehah, H.A. Aziz, S. Stoll, Nanoparticle Properties, Behavior, Fate in Aquatic Systems and Characterization Methods, J. Colloid Sci. Biotechnol. 3 (2015) 111–140, https://doi.org/10.1166/jcsb.2014.1090.
[30] K. Tai, M. Rappolt, L. Mao, Y. Gao, F. Yuan, Stability and release performance of curcumin-loaded liposomes with varying content of hydrogenated phospholipids, Food Chem. 326 (2020) 126973, https://doi.org/10.1016/j.foodchem.2020.126973.
[31] S. Li, T. Guo, W. Guo, X. Cui, M. Zeng, H. Wu, Polyphosphates as an effective vehicle for delivery of bioavailable nanoparticulate iron(III), Food Chem. 373 (2022) 131477, https://doi.org/10.1016/j.foodchem.2021.131477.
[32] S. Futaki, W. Ohashi, T. Suzuki, M. Niwa, S. Tanaka, K. Ueda, H. Harashima, Y. Sugiura, Stearylated arginine-rich peptides: A new class of transfection systems, Bioconjug. Chem. 12 (2001) 1005–1011, https://doi.org/10.1021/bc015508l.
[33] S. Ferruzza, C. Rossi, M.L. Scarino, Y. Sambuy, A protocol for differentiation of human intestinal Caco-2 cells in asymmetric serum-containing medium, Toxicol. Vitr. 26 (2012) 1252–1255, https://doi.org/10.1016/j.tiv.2012.01.008.
[34] H. Matsumoto, R.H. Erickson, J.R. Gum, M. Yoshioka, E. Gum, Y.S. Kim, Biosynthesis of alkaline phosphatase during differentiation of the human colon cancer cell line Caco-2, Gastroenterology 98 (1990) 1199–1207, https://doi.org/10.1016/0016-5085(90)90334-W.
[35] D.J. Mitchell, L. Steinman, D.T. Kim, C.G. Fathman, J.B. Rothbard, Polyarginine enters cells more efficiently than other polycationic homopolymers, J. Pept. Res. 56 (2000) 318–325, https://doi.org/10.1034/j.1399-3011.2000.00723.x.
[36] J. Pae, P. Säälik, L. Liivamägi, D. Lubenets, P. Arukuusk, Ü. Langel, M. Pooga, Translocation of cell-penetrating peptides across the plasma membrane is controlled by cholesterol and microenvironment created by membranous proteins, J. Control. Release. 192 (2014) 103–113, https://doi.org/10.1016/j.jconrel.2014.07.002.
[37] C.A. Fitch, G. Platzer, M. Okon, B.E. Garcia-Moreno, L.P. McIntosh, Arginine: Its pKa value revisited, Protein Sci. 24 (2015) 752–761, https://doi.org/10.1002/pro.2647.
[38] M. Zheng, G.M. Pavan, M. Neeb, A.K. Schaper, A. Danani, G. Klebe, O.M. Merkel, T. Kissel, Targeting the blind spot of polycationic nanocarrier-based siRNA delivery, ACS Nano 6 (2012) 9447–9454, https://doi.org/10.1021/nn301966r.
[39] G.K. Srivastava, R. Reinoso, A.K. Singh, I. Fernandez-Bueno, D. Hileeto, M. Martino, M.T. Garcia-Gutierrez, J.M. Pigazo Merino, N.F. Alonso, A. Corell, J.C. Pastor, Trypan Blue staining method for quenching the autofluorescence of RPE cells for improving protein expression analysis, Exp. Eye Res. 93 (2011) 956–962, https://doi.org/10.1016/j.exer.2011.07.002.

[40] L.I. Selby, C.M. Cortez-Jugo, G.K. Such, A.P.R. Johnston, Nanoescapology: progress toward understanding the endosomal escape of polymeric nanoparticles, Wiley Interdiscip. Rev. Nanomed. Nanobiotechnol. 9 (2017), https://doi.org/10.1002/wnan.1452.
[41] S.A. Smith, L.I. Selby, A.P.R. Johnston, G.K. Such, The Endosomal Escape of Nanoparticles: Toward More Efficient Cellular Delivery, Bioconjug. Chem. 30 (2019) 263–272, https://doi.org/10.1021/acs.bioconjchem.8b00732.
[42] C. Bechara, S. Sagan, Cell-penetrating peptides : 20 years later , where do we stand ?, 587 (2013) 1693–1702. https://doi.org/10.1016/j.febslet.2013.04.031.
[43] J.S. Appelbaum, J.R. Larochelle, B.A. Smith, D.M. Balkin, J.M. Holub, A. Schepartz, Arginine topology controls escape of minimally cationic proteins from early endosomes to the cytoplasm, Chem. Biol. 19 (2012) 819–830, https://doi.org/10.1016/j.chembiol.2012.05.022.
[44] S.L. Zackson, Enzymes and Morphogenesis: Alkaline Phosphatase and Control of Cell Migration, in: P.M. Wassarman (Ed.), Academic Press, 1993: pp. 153–183. https://doi.org/10.1016/S1566-3116(08)60029-8.
[45] J. Griesser, G. Hetényi, C. Federer, C. Steinbring, H. Ellemunter, K. Niedermayr, A. Bernkop-Schnürch, Highly mucus permeating and zeta potential changing self-emulsifying drug delivery systems: A potent gene delivery model for causal treatment of cystic fibrosis, Int. J. Pharm. 557 (2019) 124–134, https://doi.org/10.1016/j.ijpharm.2018.12.048.
[46] M. Kurpiers, J.D. Wolf, C. Steinbring, S. Zaichik, A. Bernkop-Schnürch, Zeta potential changing nanoemulsions based on phosphate moiety cleavage of a PEGylated surfactant, J. Mol. Liq. 316 (2020) 113868, https://doi.org/10.1016/j.molliq.2020.113868.